Quantum Wave Packet Dynamics with Trajectories

Courtney L. Lopreore and Robert E. Wyatt
Institute for Theoretical Chemistry, The University of Texas at Austin, Austin, Texas 78712
(Received 13 January 1999)

The de Broglie–Bohm causual (hydrodynamic) formulation of quantum mechanics is computationally implemented in the Lagrangian (moving with the fluid) viewpoint. The quantum potential and force are accurately evaluated with a moving weighted least squares algorithm. The quantum trajectory method is then applied to barrier tunneling on smooth potential surfaces. Analysis of the tunneling mechanism leads to a novel and accurate approximation: shortly after the wave packet is launched, completely *neglect* all quantum terms in the dynamical equations for motion along the tunneling coordinate. [S0031-9007(99)09563-0]

PACS numbers: 34.10.+x

Time-dependent quantum wave packets are widely used to study diverse phenomena in physics. Current computational methods for wave packet dynamics use space-time grids, basis sets, or some combination of these approaches. The goals of this study are to present a new approach to wave packet dynamics, referred to as the quantum trajectory method (QTM), and to apply this method to several problems. QTM is based upon the hydrodynamic formulation of quantum mechanics. First suggested in 1926–1927 [1,2] and later developed into a physical theory by Bohm [3] in 1952, this formulation has been the subject of a number of intepretative articles and a much smaller number of computational studies [4–7]. In this study, in order to solve the quantum hydrodynamic equations, we borrow techniques used in some areas of computational fluid dynamics (CFD). The QTM solves the equations of motion to find quantum trajectories for "fluid particles." Although particle trajectories are developed, QTM is fully quantum, and is distinct from semiclassical or classical approaches.

After presenting the dynamical equations in the "moving with the fluid" Lagrangian viewpoint, the moving weighted least squares algorithm (MWLS) is introduced for computing derivatives of a function defined on an unstructured grid. The QTM will then be applied to barrier tunneling in one and two dimensions. After elucidating the mechanism for the tunneling process, a novel approximation will be described.

The hydrodynamic formulation is initiated [1–3] by substituting the wave function $\psi(\vec{r},t) = R(\vec{r},t)e^{iS(\vec{r},t)/\hbar}$ (R and S are real valued) into the time-dependent Schrodinger equation (TDSE) and separating into real and imaginary parts,

$$\frac{\partial \rho(\vec{r},t)}{\partial t} + \vec{\nabla}\cdot\left(\rho\,\frac{1}{m}\,\vec{\nabla}S\right) = 0\,, \tag{1}$$

$$-\frac{\partial S(\vec{r},t)}{\partial t} = \frac{1}{2m}\,(\vec{\nabla}S)^2 + V(\vec{r},t) + Q(\rho;\vec{r},t)\,, \tag{2}$$

where the probability density is $\rho(\vec{r},t) = R(\vec{r},t)^2$. With identification of the velocity, $\vec{v} = \vec{\nabla}S/m$, and the flux, $\vec{j} = \rho\vec{v}$, Eq. (1) is the continuity equation. Equation (2), the *quantum Hamilton-Jacobi* (HJ) equation, is identical in form to the classical HJ equation which, however, is missing the last term. This term, the time-dependent *quantum potential* [3], is defined through the curvature of the amplitude,

$$Q(\rho;\vec{r},t) = -\frac{\hbar^2}{2m}\,\frac{1}{R}\,\nabla^2 R = -\frac{\hbar^2}{2m}\,\rho^{-1/2}\nabla^2\rho^{1/2}. \tag{3}$$

Taking the gradient of Eq. (2) leads to the equation of motion,

$$m\,\frac{d\vec{v}}{dt} = -\vec{\nabla}(V + Q) = \vec{f}_c + \vec{f}_q\,, \tag{4}$$

where the Lagrangian time derivative is $d/dt = \partial/\partial t + \vec{v}\cdot\vec{\nabla}$. In Eq. (4), there are two force terms: the "classical" force arising from the gradient of the potential surface and the *quantum force* arising from the tilt of the quantum potential.

By analogy to CFD, two paths are possible for solving the hydrodynamic equations. In the Lagrangian viewpoint, which will be followed here, solutions are obtained in a reference frame moving with the fluid. By contrast, in the Eulerian viewpoint, the equations are solved using fixed in space grids or basis sets. However, there are significant advantages to the Lagrangian "go with the flow" viewpoint. Several methods have been used to solve the Lagrangian equations in CFD, including those that define an underlying mesh so as to compute derivatives or to support basis functions. From our viewpoint, *meshless methods* [8], in which moving fluid particles serve as nodes for interpolation, are more generally applicable.

An equation in the Lagrangian viewpoint is needed to update the density. Returning to Eq. (1), we note that it may be written,

$$\left(\frac{\partial}{\partial t} + \vec{v}\cdot\vec{\nabla}\right)\rho = \frac{d\rho}{dt} = -\rho\vec{\nabla}\cdot\vec{v}\,. \tag{5}$$

The last equation may be integrated to give the updated density,

$$\rho(\vec{r},t+dt) = \Omega(t+dt,dt)\rho(\vec{r},t) = e^{-(\vec{\nabla}\cdot\vec{v})dt}\rho(\vec{r},t)\,. \tag{6}$$

 0031-9007/99/82(26)/5190(4)$15.00

Equations (4)–(6) are the Lagrangian equations of motion. In the QTM, the probability fluid is represented by N nodes or "particles" (each of mass m), which form an unstructured topology.

The MWLS algorithm provides a method for computing the derivatives needed to find the quantum potential and the quantum force. The version used here is similar to one developed for engineering and CFD applications [8,9]. Assume that a function $f(\vec{r})$ is defined on an unstructured set of points. We seek an approximate but accurate value for f in the neighborhood of point $\vec{r}_i$. In addition, there is a basis set (dimension nb) of local polynomials, $p_j(\vec{r} - \vec{r}_i)$ so that f can be expanded,

$$f(\vec{r}) = \sum_{j=1}^{\mathrm{nb}} a_j p_j(\vec{r} - \vec{r}_i). \tag{7}$$

For example, in two dimensions, if we choose the basis $B = \{1, \xi, \eta, \xi^2/2, \xi\eta, \eta^2/2, \xi^3/6, \ldots\}$, where $\xi = x - x_i$ and $\eta = y - y_i$ are local displacements, then the coefficients a_j are approximations to the function and its derivatives at this point. For example, the curvature of the function becomes $(\nabla^2 f)_i = a_4 + a_6$. In order to find the $\{a_j\}$, we require that the approximation in Eq. (7) passes through np points near point $\vec{r}_i$ (these points form the *stencil* or *star*),

$$f(\vec{r}_k) = \sum_{j=1}^{\mathrm{nb}} a_j p_j(\vec{r}_k - \vec{r}_i), \qquad k = 1, 2, \ldots, \mathrm{np}. \tag{8}$$

To solve these equations in the least squares sense, we require that np $>$ nb. In addition, each equation is assigned a weight $w(r_{kl})$ depending upon the distance r_{kl} between points k and l (a Gaussian is used in practice). Error minimization criterion for the coefficients $\{a_j\}$ then leads to an equation for the solution vector **a** (dimension nb $\times$ 1) in terms of the known function vector **f** (np $\times$ 1). The result is that *the derivatives of f can be expressed in terms of the known function values for points in the star*. For example, the curvature can be expressed,

$$(\nabla^2 f)_i = \sum_{k=1}^{\mathrm{np}} \Omega_{ik} f(\vec{r}_k). \tag{9}$$

An equation analogous to Eq. (9) was used to evaluate Q, $\vec{f}_q$, and $\vec{\nabla} \cdot \vec{v}$ (for updating the density). For the applications that will be described, nb = 6 and np = 20–30. It should be noted that the MWLS algorithm can break down when the particles move far apart, but in practice this happens after useful physical information has been extracted.

The QTM will now be applied to tunneling through one and two dimensional smooth potential barriers. In the first analysis based upon the Bohmian viewpoint, Dewdney and Hiley [5] studied the scattering of Gaussian wave packets from rectangular barriers. Commenting on this study, Bohm and Hiley [10] (BH) stated "In general, the quantum potential will lower the barrier height, thus permitting particles to enter it. This, of course, removes the mystery as to how barrier penetration is possible. For such penetration depends on the total potential $V + Q$ and not just the classical potential alone." Also regarding this study, Holland wrote [11] "...the effects come about from the modification of the total energy of each particle...*in the vicinity of the barrier* (italics added)." The picture presented by BH is quite appealing: as particles approach the barrier, the effective barrier lowers (due to the quantum potential), thus allowing some of the particles to slip through. When the "right number" makes it to the other side, the effective barrier raises and the lagging particles are forced away. Surprisingly, we will see for smooth barrier penetration that *this view is misleading and incorrect.*

We first consider the one dimensional scattering of a Gaussian wave packet (GWP) from the Eckart potential, $V(x) = V_0 \,\mathrm{sech}^2[a(x - x_b)]$, where V_0 is the barrier height and "a" measures the barrier width. In these studies, $V_0 = 8000\ \mathrm{cm}^{-1}$, $x_b = 6$ a.u., and $a = 0.5$ a.u. The initial GWP is $(2\beta/\pi)^{1/4} \exp\{-\beta(x - x_0)^2 + ikx\}$, where $\beta = 10$ a.u., the translational energy is $E = \hbar^2 k^2/2m$, with E in the range 10 to 12 000 cm^{-1}, and $m = 2000$ a.u. The initial condition for the speed of each particle is $v = \hbar k/m$. At $t = 0$, the N particles are centered at x_0 and distributed with a spacing 0.04 a.u. The particle ensemble, with N in the range 21–51, was then propagated with time steps of 2 a.u. (0.048 fs).

The time-dependent reaction (transmission) probability was computed by integrating ρ on the product side of the barrier, $x > x_b$. At late times, this probability approaches the value denoted $P(E)$; see Fig. 1. The points show the energy dependence computed with the QTM (N = 51), and the continuous curve shows the exact probability obtained from numerical integration of the TDSE. *The remarkable feature is that over almost 4 orders of*

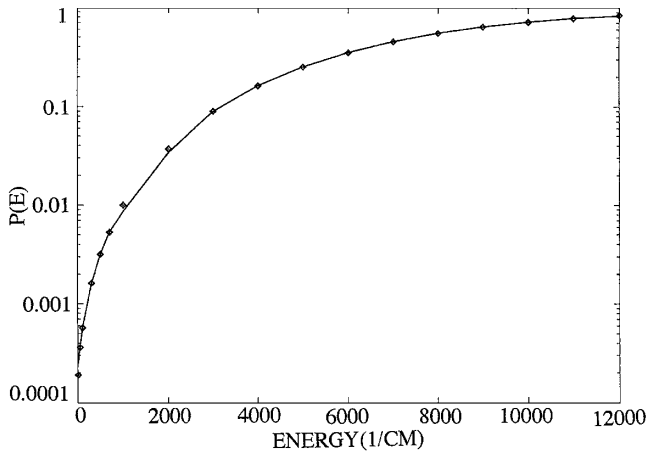

FIG. 1. Energy dependence of the transmission probability for an Eckart barrier with a height $V_0 = 8000\ \mathrm{cm}^{-1}$. The points were obtained using the quantum trajectory method with $N = 51$, and the continuous curve shows exact results from the numerical integration of the TDSE.

magnitude, the QTM with a small number of trajectories yields tunneling probabilities in excellent agreement (the errors range from <1% to 3% at the plotted points) with the exact results.

We will now focus on the tunneling mechanism at one initial energy, $E = (3/4)V_0$. In this case, the leading 24 particles (No. 28–51) make it to the product region, while the lagging 27 particles eventually form the reflected packet. There is thus a bifurcation in the dynamics between trajectories 27 and 28. Why does No. 28 make it through whereas No. 27 fails to make the grade? The answer is provided in Fig. 2. First, the time dependencies of the kinetic energies (KE) for these two trajectories are shown in part (a). At $t = 0$, both trajectories have the same KE, but just after launching, *both particles acquire KE during the boost phase.* At about 4 fs, both particles begin the *deceleration phase* as they ascend the outer edge of the barrier. For No. 27, deceleration continues until a turning point is reached at 28 fs. The potential at this point is $V = 7600$ cm^{-1}; particle 27 almost made it over the top. After 28 fs, this particle rolls back down the potential hill, picking up KE along the way. Particle 28, however, decelerates from 4 until 25 fs, at which time it skims over the top of the barrier with about 500 cm^{-1} of "excess" KE. It then accelerates down the product side of the barrier. There is an important lesson: particle 28 made it over the top of the hill, *because it picked up sufficient KE in the first few femtoseconds of flight.* For every particle lagging behind this one, the KE boost is insufficient to give enough "kick" to make it over the hill. Clearly, the customary phrase "tunneling through the barrier" is both misleading and incorrect; *the particles "tunnel" by skimming over the top of the barrier with positive KE at all times.*

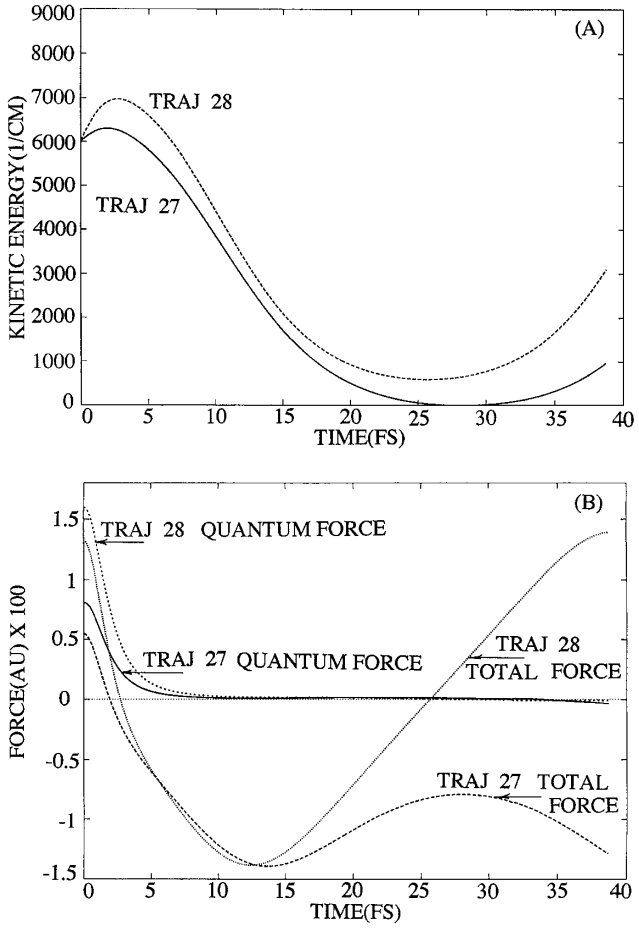

FIG. 2. Trajectory analysis at the initial translational energy $E = (3/4)V_0$. (a) Kinetic energy vs time for trajectories 27 (nonreactive) and 28 (reactive). (b) Total force and quantum force vs time for these trajectories.

It is also instructive to examine both the quantum and total forces for these two trajectories; see Fig. 2(b). For both trajectories, the positive accelerating force for 3–4 fs (the boost phase) then gives way to the deceleration phase. Particle 28 experiences no force as it crosses the crest of the hill at 25 fs; after that, it accelerates down the product side of the potential. By contrast, particle 27 reaches a local minimum in the force at 28 fs (the turning point), then accelerates back downhill with $f_{\text{total}} < 0$. This figure shows the important accelerating influence of the quantum force at early times. However, *after about 8–10 fs, the role played by f_q is completely negligible.*

The origin of the boost phase may be understood by considering the quantum force for a freely evolving GWP [11]: $f_q(x) = (4\beta^2/m)(x - x_0)$, where β and x_0 are functions of time. Note that particles on the leading edge feel a positive force; those on the trailing edge feel a negative force. As a result, the particles move apart, thus producing wave packet spreading. In addition, particles more distant from the center experience the largest acceleration (if $x > x_0$) or deceleration (if $x < x_0$). Returning to the barrier tunneling example described previously, particle 28 is located slightly "ahead" of particle 27, so at early times it receives the larger accelerating force during the boost phase. Although not explicitly considered here, the same tunneling mechanism applies at other energies.

A dynamical approximation is suggested by this tunneling mechanism. Since $\vec{f}_q$ plays a significant role only during the boost phase, let the initially prepared wave packet evolve for a short time (up to the *decoupling time*, t_d), then *turn off the quantum force before the particles enter the barrier region.* This scheme is the *decoupling approximation.* For $t > t_d$, the particles evolve as a classical ensemble. Of course, if t_d is too short, the leading particles do not have sufficient time to be boosted to energies sufficient to surmount the barrier. For the case described previously with $t_d = 7.7$ fs, $P(E) = 0.345$, which is close to the exact value (0.352).

The QTM can be readily extended to multidimensional problems. An application in two dimensions will be considered. The model potential, expressed in (x, y) coordinates, is an Eckart barrier along x and a harmonic trough along y, where the force constant for the harmonic

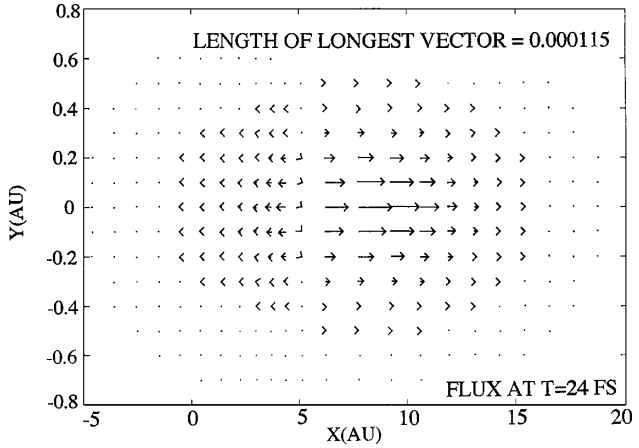

FIG. 3. Flux map obtained using the quantum trajectory method for an Eckart barrier-harmonic potential surface (dots locate the 297 particles). Flux vectors with lengths below a threshold value were not plotted. At $t = 0$, the wave packet was centered at the point $(2, 0)$ with the barrier maximum at $(6, 0)$.

potential is $k = 0.191$ a.u. The wave packet at $t = 0$ is the product of a GWP times a ground state harmonic oscillator function for the y mode. At a series of energies, flux maps were made at various times during the scattering process. For example, Fig. 3 shows the flux map at $t = 24$ fs for the initial energy $E = (3/4)V_0$ with 297 particles in the ensemble. Near the barrier maximum the flux is dividing into reactive and reflected components. In this calculation, a decorrelation time $t_d = 9.7$ fs was used for the tunneling mode (only). The length of the longest vector differs by 2% from the value obtained when the full quantum force was used for both modes.

The computational effort in the QTM calculation scales with the number of particles approximately as $N^{1.2}$ (for $N < 10^3$). For the relatively small number of cases where we have experience, the QTM is faster than conventional wave packet propagation. Future investigations will analyze the viability of QTM for multidimensional problems where conventional wave packet propagation is not possible.

In summary, some features of the quantum trajectory method are as follows: (1) The only approximation involves the use of a finite number of particles, but accurate results can be obtained with a small number of trajectories; (2) a Lagrangian (moving) self-adaptive nodal structure is utilized; (3) there are no basis set expansions, fixed spatial grids, or absorbing potentials at the edges of grids; (4) only real-valued trajectories and energies are used, even for classically forbidden barrier tunneling; (5) the method and the computer codes can be readily extended to more dimensions; (6) for each degree of freedom, full quantum, partial quantum, or classical calculations can be performed by scaling the quantum force.

This work was supported in part by the National Science Foundation and the Robert Welch Foundation of Houston, Texas.

[1] L. de Broglie, C. R. Acad. Sci. Paris **183**, 447 (1926); **184**, 273 (1927).
[2] E. Madelung, Z. Phys. **40**, 322 (1926).
[3] D. Bohm, Phys. Rev. **85**, 166 (1952); **85**, 180 (1952).
[4] J. H. Weiner and Y. Partom, Phys. Rev. **187**, 1134 (1969); Phys. Rev. B **1**, 1533 (1970); J. H. Weiner and A. Askar, J. Chem. Phys. **54**, 1108 (1971); **54**, 3534 (1971); A. Askar and J. H. Weiner, Am. J. Phys. **39**, 1230 (1971).
[5] C. Dewdney and B. J. Hiley, Found. Phys. **12**, 27 (1982).
[6] P. Zimmerer, M. Zimmermann, N. Grun, and W. Scheid, Comput. Phys. Commun. **63**, 21 (1991).
[7] B. K. Day, A. Askar, and H. Rabitz, J. Chem. Phys. **109**, 8770 (1998).
[8] T. Belytschko, Y. Krongauz, D. Organ, M. Fleming, and P. Krysl, Comput. Methods Appl. Mech. Eng. **139**, 3 (1996).
[9] T. Liszka, Int. J. Numer. Methods Eng. **20**, 1599 (1984); T. J. Liszka, C. A. M. Duarte, and W. W. Tworzydlo, Comput. Methods Appl. Mech. Eng. **139**, 263 (1996).
[10] D. Bohm and B. J. Hiley, *The Undivided Universe* (Routeledge, London, 1993).
[11] P. R. Holland, *The Quantum Theory of Motion* (Cambridge, New York, 1993).